THE JOURNAL OF PHYSICAL CHEMISTRY C

Article

Cite This: J. Phys. Chem. C 2019, 123, 27997−28007

pubs.acs.org/JPCC

Transmission Line Model for Description of the Impedance Response of Li Electrodes with Dendritic Growth

Sara Drvarič Talian,[†] Jernej Bobnar,[†] Anton Rafael Sinigoj,[‡] Iztok Humar,[‡] and Miran Gaberščček*[,†,§]

[†]National Institute of Chemistry, 1000 Ljubljana, Slovenia

[‡]Faculty of Electrical Engineering, University of Ljubljana, Tržaška cesta 25, 1000 Ljubljana, Slovenia

[§]Faculty of Chemistry and Chemical Technology, University of Ljubljana, Večna pot 113, 1000 Ljubljana, Slovenia

Supporting Information

ABSTRACT: A general transmission line model that is able to describe accurately the measured impedance spectra of uncycled and cycled lithium electrodes is introduced. The model has all the essential features that are contained in analytical solutions for determining the impedance response of porous electrodes. In addition to that, it allows easy coupling between the various phenomena met in lithium anodes in contact with a separator: transport through a solid electrolyte interphase film, transport across "live lithium dendrites", reaction inside "live lithium dendrites", transport across "dead dendrites", diffusion in a porous separator, and so forth. The model is used for quantitative analysis of measured impedance spectra collected at different C-rates and after different numbers of charge−discharge cycles. Further, combining impedance spectroscopy with scanning electron microscopy, several unique correlations between the morphological development of lithium anodes and development of impedance spectra are identified and discussed. Finally, several simplified schemes that allow identification of the main degradation or failure mechanism(s) occurring in cycled lithium anodes are presented.

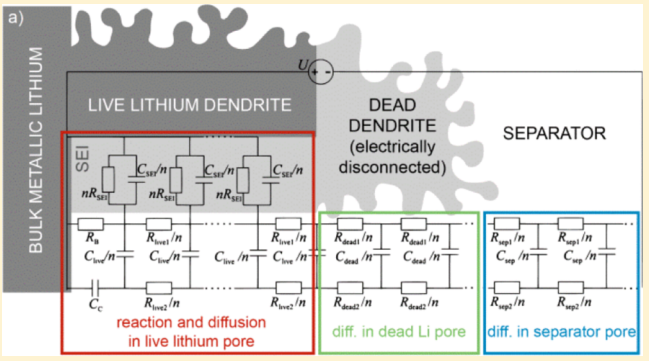

1. INTRODUCTION

Metallic lithium has been used as the anode in lithium batteries for more than 40 years.[1,2] Its stability in organic electrolytes is connected to spontaneous formation of a passive surface layer that effectively prevents further electronic interaction with the electrolytes. On the other hand, this layer conducts lithium ions; hence, it has widely been known as the solid electrolyte interphase (SEI). The detailed composition and morphology of the spontaneously formed SEI strongly depend on the electrolyte used.[3−5] Furthermore, both features can change significantly when the lithium anode is discharged—as found in many studies related to the behavior of primary lithium batteries.[6−9] The nature of the SEI changes even more dramatically upon repetitive charging−discharging (cycling) of lithium.[10−12] The latter may lead to formation of special surface structures such as dendrites, large relative volume changes during cycling, high Li reactivity, electrolyte dry out, and, ultimately, occurrence of a short circuit between anodes and cathodes. Exciting new approaches have been proposed recently, for example, operando video microscopy, which have helped additionally resolve the complex behavior of Li anodes during operation.[13] A better understanding of these phenomena is essential for further development of advanced rechargeable batteries based on Li anodes, such as lithium−sulfur or lithium−air (oxygen) battery systems.

In this work, we try to get a better insight into the dynamics of lithium surface processes during cycling by introducing an appropriate impedance model that describes all the essential transport reaction features that may occur in cycled lithium anodes. A special focus is given to the occurrence and growth of porous active lithium dendrites as well as the occurrence of the so-called "dead Li dendrite layer" during progressive cycling of Li under various conditions of interest. The model takes advantage of the flexibility of the transmission line approach. Thus, we demonstrate how the transmission line evolves from a simpler version that well describes the uncycled lithium into a more complex transmission line scheme after a certain number of charge−discharge cycles (cf. Figures 4 and 5). Furthermore, the present transmission line approach allows for a rather easy coupling between the transport in the porous parts of a surface film and the transport in the bulk electrolyte phase.[14] This is essential for the present purposes as we directly compare the outcome of modeling with the actual impedance measurements, where one cannot avoid the contribution of a bulk electrolyte (i.e., an electrolyte within the porous separator that separates both electrodes).

Received: June 21, 2019
Revised: October 19, 2019
Published: October 29, 2019

DOI: 10.1021/acs.jpcc.9b05887
J. Phys. Chem. C 2019, 123, 27997−28007

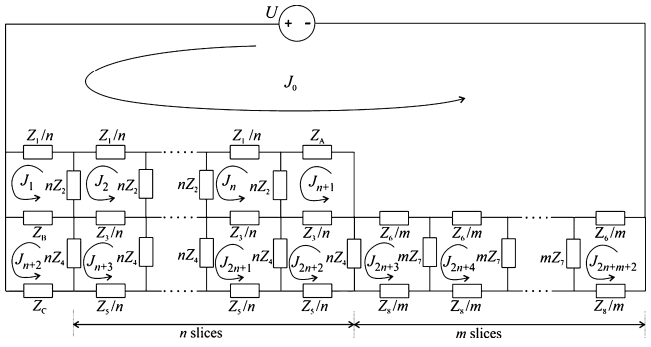

Figure 1. General transmission line having typical features of transmission lines used in the present paper. The left section divided into n slices corresponds to a porous electrode containing an active material on the surface of which the electrochemical reaction occurs (elements Z_2). The right section divided into m slices describes the chemical diffusion in an adjacent porous material in which no reaction occurs (e.g., separator, SEI film, etc.). U is a voltage source, whereas J_i represents the loop currents used for the calculation of impedance (see the main text).

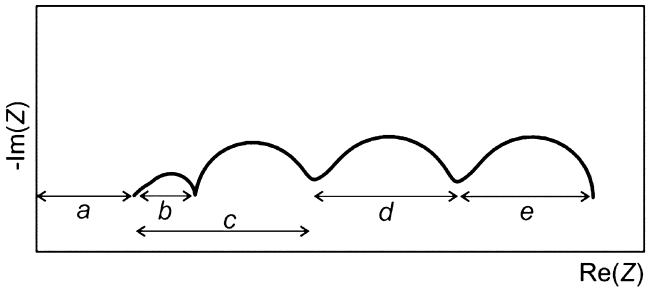

Figure 2. General shape of the impedance spectrum for the model shown in Figure 5 (see Results and Discussion). The indicated sections correspond to resistance formulas as shown below. The indexes of resistances are denoted and explained in Figure 5 and the corresponding text. *Note: Although eqs B2 and B3 are approximate, they can act as good guidelines for the estimation of the corresponding sections a and b in the complex plane representation.

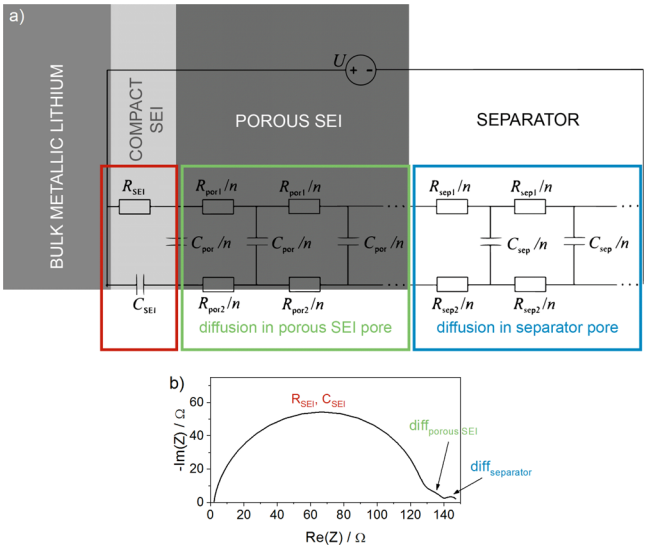

Figure 4. Pristine (uncycled) lithium in contact with an electrolyte: (a) proposed transmission line model and (b) typical corresponding impedance spectrum with denoted main processes. "diff" stands for "diffusion in ...".

As shown in the Results and Discussion section, the present transmission line approach is able to describe the measured features quite accurately, even in cases where unconventional shapes of spectra are observed. Importantly, all the elements used in the transmission line model have a clear physical background. Thus, knowing the geometry of various surface layers (thickness, surface area, etc.), one can rather directly extract the appropriate transport/reaction parameters such as chemical diffusion coefficient, concentration of mobile carriers, exchange current density, capacity of SEI layer, and so forth. In the last part of the paper, we present a couple of analyses that demonstrate the unprecedented insight into possible morphological development of a lithium surface based on a combination of microscopical observation of the Li surface, impedance measurements, and impedance modeling. Finally, we discuss possible qualitative and quantitative criteria that may be used for

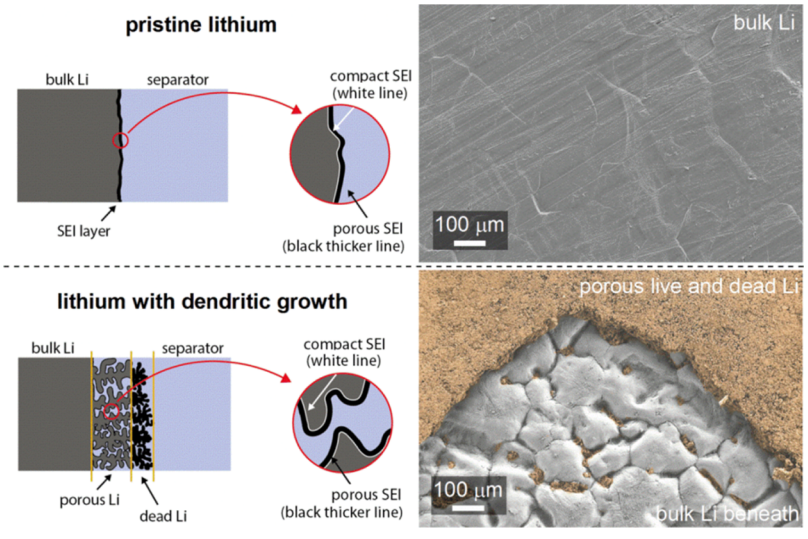

Figure 3. Graphical representation and corresponding SEM images of pristine Li electrode and Li electrode with dendritic growth causing a layer of porous and dead Li dendrites on top of the bulk electrode (shown in color on the SEM micrograph—the image was taken on a part of the electrode, where the dendritic layer detached from the Li electrode).

DOI: 10.1021/acs.jpcc.9b05887
J. Phys. Chem. C 2019, 123, 27997−28007

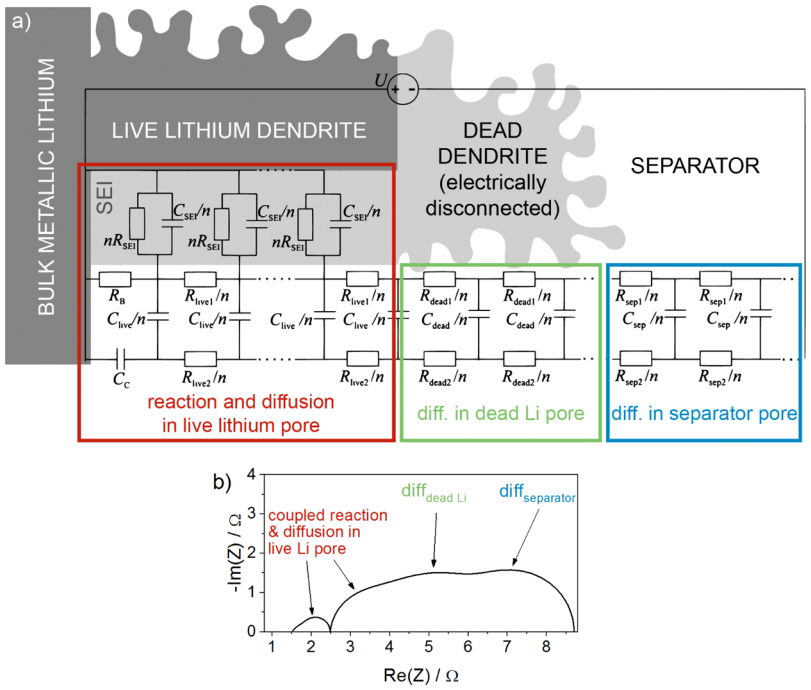

Figure 5. Proposed transmission line model used to describe the impedance spectra of lithium electrodes with dendritic growth: (a) schematic representation of the different parts of the transmission line model corresponding to the redox reaction/SEI contribution and three different diffusional "environments" (live lithium pore, dead lithium pore, and separator); note that the interaction of species with the walls of live lithium is simplified—the transport across the porous part of SEI is neglected (unlike in Figure 4); the electrochemical reaction of lithium is also neglected, as in Figure 4; (b) an example of an impedance spectra simulated with the transmission line model. "diff" stands for "diffusion".

rough identification of main scenarios (e.g., growth of live dendrites, excessive growth of dead lithium, electrolyte dry out, etc.), leading to degradation/failure of the given lithium anode during cycling.

2. EXPERIMENTAL SECTION

2.1. Cell Assembly. Lithium symmetrical cells were assembled inside an MBRAUN glovebox, in which oxygen and water contents were held below 1 ppm. The electrodes were punched out as 2 cm^2 circles out of a 110 μm ribbon (FMC, USA). No pretreatment was carried out on the Li surface before cell assembly. The cells were assembled in Triplex pouch cells with nickel contacts by stacking two lithium electrodes with a Celgard 2320 separator between them. The separator was wetted with 20 μL of 1 M LiTFSI in the TEGDME/DOL 1:1 (v/v) electrolyte before sealing the pouch. The electrolyte solution was prepared from previously dried LiTFSI (Sigma-Aldrich, dried under vacuum at 140 °C overnight), tetraglyme (TEGDME, Acros, dried using molecular sieves, K/Na alloy, and distillation), and 1,3-dioxolane (DOL, Sigma-Aldrich, dried using molecular sieves, K/Na alloy, and distillation).

2.2. Electrochemical Experiments. The electrochemical experiments on the cells were done with a combination of impedance spectroscopy measurements and stripping and deposition cycles on Li||Li symmetrical cells. The cells were connected to a VMP3 Biologic potentiostat/galvanostat within 10 min of cell assembly. The cells were then left to stabilize for 24 h, during which impedance spectra were measured. After this initial period, the Li||Li cells underwent stripping and deposition at a constant current rate with each half-cycle lasting for 2 h. The exact number of cycles and the current rate used varied and is given with each figure. The current for the discharge/charge cycles was either 0.2 mA ("low current cells") or 1.0 mA ("high current cells"). After stripping and deposition of lithium, the cells were left to relax for 15 min, after which impedance spectra were measured. All of the impedance spectroscopy measurements were done in the range of 1 MHz to 1 mHz with an amplitude voltage of 10 mV (rms).

2.3. Morphological Analysis. The Li electrode surface after the cycling experiment was examined with a scanning electron microscope (FESEM, SUPRA 35VP, Zeiss, Germany). For this purpose, cells were disassembled inside the glovebox and the electrodes were washed with dry DOL to remove any salt residue on the surface. The samples were transferred to the scanning electron microscope by sealing them in a vacuum holder, which was opened inside the microscope chamber, to avoid contact with the atmosphere. The accelerating voltage for scanning electron microscopy (SEM) analysis was 1.5 kV.

3. THEORETICAL SECTION

3.1. Procedure for the Present Transmission Line Model. First, we briefly describe the method used for calculating the impedance response of present transmission lines. We used the well-known mesh method which assigns the so-called mesh currents in the essential meshes of the circuit. In Figure 1, such independent meshes can be identified by the corresponding loop currents J_i. Specifically, in the present case, one can identify $2n + m + 3$ independent meshes corresponding to loop currents J_0 to J_{2n+m+2} (see Figure 1).

According to Kirchhoff's voltage law, the following equations can be constructed for individual meshes

DOI: 10.1021/acs.jpcc.9b05887
J. Phys. Chem. C 2019, 123, 27997−28007

$$[n(Z_1/n) + Z_A + m(Z_6/m)]J_0 - (Z_1/n)J_1 - (Z_1/n)J_2 - \ldots - (Z_1/n)J_n - Z_AJ_{n+1} - (Z_6/m)J_{2n+3} - (Z_6/m)J_{2n+4} - \ldots - (Z_6/m)J_{2n+m+2} = U \quad (A0)$$

$$-(Z_1/n)J_0 + (Z_1/n + Z_B + nZ_2)J_1 - (nZ_2)J_2 - Z_BJ_{n+2} = 0 \quad (A1)$$

$$-(Z_1/n)J_0 - (nZ_2)J_1 + (Z_1/n + Z_3/n + 2nZ_2)J_2 - (nZ_2)J_3 - (Z_3/n)J_{n+3} = 0 \quad (A2)$$

$$-(Z_1/n)J_0 - (nZ_2)J_{n-1} + (Z_1/n + 2nZ_2 + Z_3/n)J_n - (nZ_2)J_{n+1} - (Z_3/n)J_{2n+1} = 0 \quad (An)$$

$$-Z_AJ_0 - (nZ_2)J_n + (Z_A + nZ_2 + Z_3/n)J_{n+1} - (Z_3/n)J_{2n+2} = 0 \quad (An+1)$$

$$-Z_BJ_1 + (Z_B + Z_C + nZ_4)J_{n+2} - (nZ_4)J_{n+3} = 0 \quad (An+2)$$

$$-(Z_6/m)J_0 - (nZ_4)J_{2n+2} + (Z_6/m + nZ_4 + Z_8/m + mZ_7)J_{2n+3} - (mZ_7)J_{2n+4} = 0 \quad (A2n+3)$$

$$-(Z_6/m)J_0 - (mZ_7)J_{2n+m+1} + (Z_6/m + mZ_7 + Z_8/m)J_{2n+m+2} = 0 \quad (A2n+m+2)$$

Using the above set of $2n + m + 3$ equations, one can uniquely determine the $2n + m + 3$ unknown loop currents J_i. The impedance of transmission line is then readily calculated as U/J_0.

In most of the present simulations, we typically used 200 slices for each model section, that is, 200 for the porous active electrode ($n = 200$) and 200 for the porous SEI film ($m = 200$). In addition, further 200 slices were added because of diffusion in the separator (not shown in the Theoretical Section but clearly indicated in Figure 5). Occasionally, we also checked the simulation outcomes for up to 2000 slices. The average error of calculated impedance values for discretization into 200 slices was estimated to be in the range 0.1−1%, depending on the parameter values and the frequency used. In any case, this is much below the estimated experimental error (on the order of 5−10%). The error was determined by comparing the results of the present mesh method with the values from the exact solution (the latter is available for a basic transmission line as discussed in our previous paper[15]).

3.2. General Features of Simulated Spectra in the Case of 100% Coverage of Li with Dendrites (See the Model Shown in Figure 5).

$$a = \frac{R_{dead1}R_{dead2}}{R_{dead1} + R_{dead2}} + \frac{R_{sep1}R_{sep2}}{R_{sep1} + R_{sep2}} \quad (B1)$$

$$b = \sqrt{R_{par}R_{SEI}}\coth\sqrt{R_{par}/R_{SEI}} \quad (B2)$$

*where $R_{par} = \frac{R_{live1}R_{live2}}{R_{live1} + R_{live2}}$

$$c = \sqrt{R_{live1}R_{SEI}}\coth\sqrt{R_{live1}/R_{SEI}} \quad (B3)$$

*

$$d = R_{dead1} - \frac{R_{dead1}R_{dead2}}{R_{dead1} + R_{dead2}} \quad (B4)$$

$$e = R_{sep1} - \frac{R_{sep1}R_{sep2}}{R_{sep1} + R_{sep2}} \quad (B5)$$

$$R_{total} = a + c + d + e = \sqrt{R_{live1}R_{SEI}}\coth\sqrt{R_{live1}/R_{SEI}} + R_{dead1} + R_{sep1} \quad (B6)$$

3.3. General Formulas Assumed upon Construction of the Present Transmission Line.

The parameters of the present transmission line can be uniquely linked to selected parameters with clear physical meaning as known from electrochemical modeling on the continuum level. For example, if we assume a system of two mobile carriers (having indexes 1 and 2) in an unsupported system, the following equations may be constructed[16]

$$R_1 = \frac{L}{A}\frac{RT}{F^2}\left(\frac{1}{z_1^2 c_{Li^+}D_{Li^+}}\right) \quad (C1)$$

$$R_2 = \frac{L}{A}\frac{RT}{F^2}\left(\frac{1}{z_2^2 c_{anion}D_{anion}}\right) \quad (C2)$$

$$C_{chem} = LA\frac{F^2}{RT}\left(\frac{1}{z_1^2 c_{Li^+}} + \frac{1}{z_2^2 C_{anion}}\right)^{-1} \quad (C3)$$

where R_1 and R_2 are general migration resistances for mobile carrier 1 and 2 (e.g. Li ions and counter anions), respectively, L is the length of space in which migration and diffusion occur, A is the geometrical surface area of the electrode, R is the gas constant, T is the temperature, F is Faraday's constant, z_1 and z_2 are the number of unit charges on cations and anions, respectively (we assume $z_1 = z_2 = 1$), c_{Li^+} and c_{anion} are the respective concentrations of both mobile charges, and D_{Li^+} and D_{anion} are their diffusivities, respectively.

The corresponding chemical diffusion coefficient of such a two-charge system reads

$$D_{chem} = \frac{L^2}{(R_1 + R_2)C_{chem}} \quad (C4)$$

whereas the transport number for species 1 (Li ion) is

$$t_1 = \frac{R_2}{R_1 + R_2} \quad (C5)$$

It is necessary to point out that although this paper considers porous electrodes, the porosity itself is not treated as a separate parameter. Rather, it appears as an implicit prefactor to chemical diffusion coefficient. Thus, D_{chem} in eq C4 should be considered an effective chemical diffusion coefficient. Consequently, if porosity changes, D_{chem} will also change even if C4 does not contain porosity explicitly.

3.4. Analysis of Measurements Using the Present Model.

As indicated in sections 3.2 and 3.3, the basic elements of the present model are local capacitors and resistors that have a

DOI: 10.1021/acs.jpcc.9b05887
J. Phys. Chem. C 2019, 123, 27997−28007

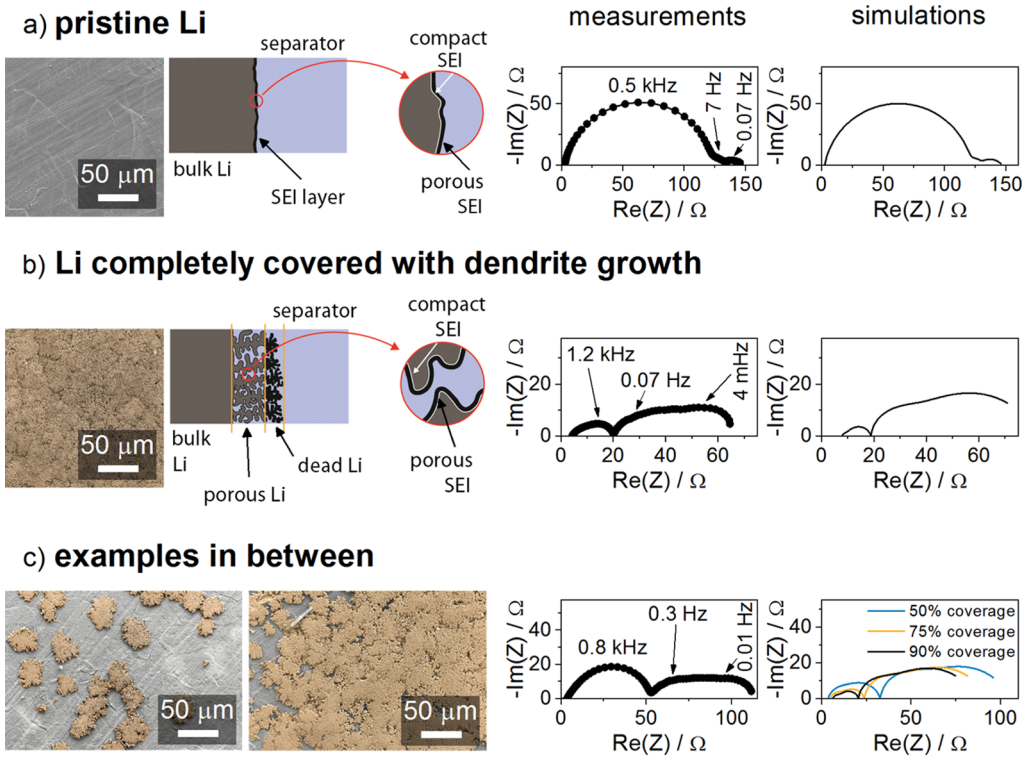

Figure 6. Three different cases distinguished in experiments described with SEM micrographs, a simple graphical representation, impedance spectra measurements, and impedance spectra simulations using a transmission line model describing dendritic growth: (a) pristine Li electrode (the spectrum was measured on a pristine Li symmetrical cell after 24 h of stabilization at open-circuit voltage), (b) Li electrode completely covered with dendrites (the spectrum was measured on a Li symmetrical cell after 40 cycles of stripping and deposition at ±0.1 mA cm^2 current), and (c) examples in between the cases shown in (a,b), namely, where dendrites were present as individual islands covering the bulk electrode to a different degree (the spectrum was measured on a Li symmetrical cell after 20 cycles of stripping and deposition at ±0.1 mA cm^2 current).

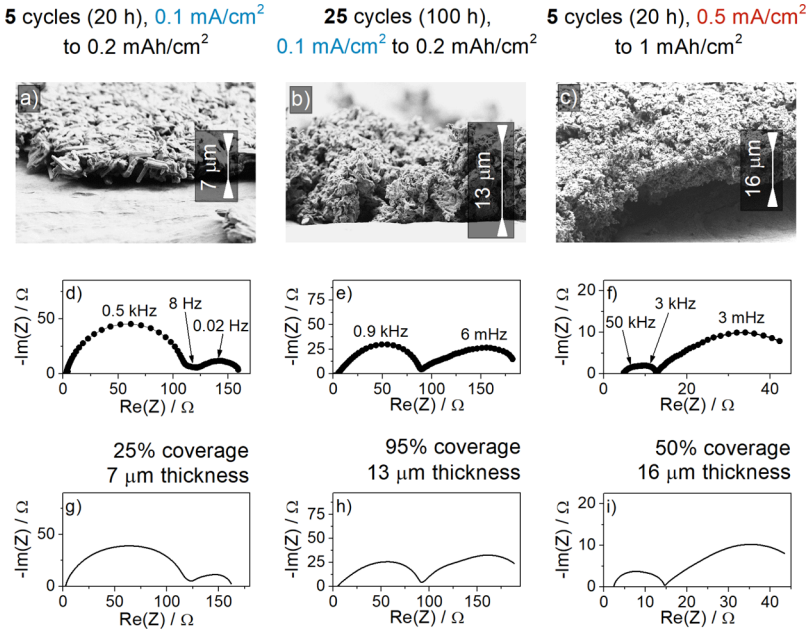

Figure 7. Li electrode micrographs and impedance spectra after different numbers of cycles of stripping and deposition at 0.1 and 0.5 mA cm^{-2} current density: (a−c) SEM micrographs showing the thickness of the porous and dead Li layer on the surface, (d−f) impedance spectra measured after the stated electrochemical experiment, and (g−i) simulation using transmission line model assuming the stated degree of coverage and thickness of the dendritic layer; in all cases, the simulated spectra have the same peak frequencies as the measured ones.

clear physical background as indicated by the respective equations. However, it is noted that the measured spectra cannot be accurately fitted with the proposed model. The problem is that the measured shapes deviate from the theoretically predicted ones quite significantly. It is well known in the impedance spectroscopy community that this

DOI: 10.1021/acs.jpcc.9b05887
J. Phys. Chem. C 2019, 123, 27997−28007

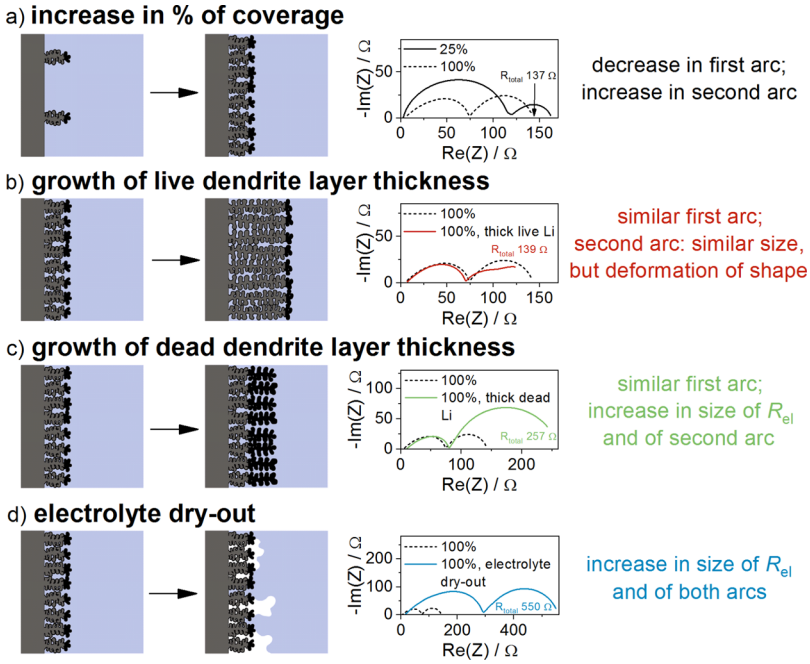

Figure 8. Change of impedance response upon different scenarios of dendrite growth. (a) Effect of increase of surface coverage, (b) effect of increasing the thickness of live dendritic lithium, (c) effect of increasing the thickness of dead dendritic lithium, and (d) effect of electrolyte dry out. The values of total electrode resistance (R_{total}, see eq B6) are given next to each spectrum.

issue can be removed by replacing the capacitive elements with the so-called constant-phase elements (CPEs) using the following equation

$$\mathrm{CPE}_k = 1/(\mathrm{j}\omega)^{\alpha k} Q_k \tag{D1}$$

where Q_k replaces the corresponding capacitive element C_k and αk has a value between 0 and 1.

We note, however, that the physical origin of CPEs is unclear in the present case. Additionally, we have found that in cases when different processes (different arcs) strongly overlap—such as in the present case—any use of CPE_k instead of C_k may significantly distort the general shape of the major low-frequency spectra which complicates the determination of individual parameters. More importantly, the value of αk may have rather pronounced effect not only on the shape of the spectra but also on the value of Q_k. Thus, fitting a series of measured spectra using CPE_k may lead to physically unsound trends of Q_k if αk changes significantly.

Based on the above considerations, we tried to avoid the use of CPE elements whenever possible. This however meant that we had to refrain from fitting of the measured spectra. Instead, we decided to implement an alternative approach frequently used a couple of decades ago in the field of corrosion.[17,18] Specifically, we carried out a number of sets of measurement by changing the given parameter, that is, cycle number or cycling rate. This way, we obtained many hundreds of measurements that showed certain trends, some of which were quite reproducible. Then, we performed extensive sensitivity analysis of the proposed model (thousands of simulations) in order to establish a correlation between the model parameters and the observed reproducible experimental trends. In this sensitivity analysis, we only used the physical parameters—that is, no CPE elements were involved. Beside the trends of shapes, the trends of quantitative data extracted from the spectra (peak frequencies, size of arcs, size of high-frequency intersection, etc.) were carefully considered. Based on this comprehensive analysis, we could identify certain patterns and dependencies that acted as a basis for creation of scenarios as shown in Figure 8.

Finally, we note that although the whole sensitivity analysis was carried using capacitances rather than CPE elements, we occasionally carried out additional simulations in which capacitances were replaced by CPEs. By doing so, the simulated spectra also became visually very similar to the measured spectra. We also used such replacements in some of the present figures (e.g., Figures 6–8)—in order to demonstrate that the present model can reproduce the measured shapes in significant detail.

4. RESULTS AND DISCUSSION

Pristine (uncycled) metallic lithium electrode is supposed to have a rather smooth surface (see the upper part of Figure 3) covered with an SEI layer. This layer may be morphologically and compositionally complex, consisting of various organic and inorganic Li compounds formed during lithium metal production and those formed by chemical reaction upon the contact of the electrode with the electrolyte. For the present purposes, it is convenient to somewhat simplify the actual features and divide the SEI layer into two limiting parts: a thin (several nanometers), compact (pore-free) SEI sublayer that is attached tightly to the metal and a porous thicker SEI layer (up to the micrometer range) that grows at the electrolyte side (Figure 3, top).[4] The transport across the thin compact sublayer primarily consists of migration of Li^+ ions (these are the only mobile species in the solid structure of SEI). By contrast, the transport across the porous thicker part of SEI is mainly realized through the liquid electrolyte in the pores. Thus, migration of both mobile species (lithium ions and negative ions in electrolyte phase) is possible, as well as their coupled (chemical) diffusion.

During repetitive charge and discharge (cycling) of Li metal anodes, special surface structures usually called dendrites are formed on the previously rather smooth surface (compare top

DOI: 10.1021/acs.jpcc.9b05887
J. Phys. Chem. C 2019, 123, 27997−28007

and bottom of Figure 3). The dendrites are a result of repetitive dissolution and stripping of lithium into/from bulk solution whereby these processes do not proceed uniformly across the whole surface but locally on energetically most convenient sites. Thus, instead of uniform "thinning and thickening" of lithium anodes, one observes a patch-like growth and dissolution of dendrites across selected anode regions. Eventually, during prolonged cycling, these patches merge into a continuous and progressively thicker surface formation (see, e.g., the bottom right micrograph in Figure 3). In some cases, the patches may also grow preferentially in the perpendicular direction forming needlelike structures that can short circuit the anode and cathode. In any case, during each cycle, the newly deposited lithium metal quickly passivates because of the contact with the electrolyte, forming an SEI layer on the surface of the dendrites, similar to the SEI found in the pristine lithium upon cell assembly.

Although dendrites are a result of complex dissolution, growth and passivation processes occurring during cycling, many previous studies[19−22] have offered good indications of their typical structure, as shown in Figure 3 (bottom left). Specifically, we may divide a dendrite into two, essentially porous layers: (i) the so-called "live porous lithium" whose surface is covered with SEI but still contains sufficient amount of Li to maintain electronic connection to the bulk lithium and (ii) "dead porous lithium" which is electronically and ionically disconnected from the bulk lithium because of excessive passivation and interruption of eventual conductive paths leading to bulk lithium; alternatively, "dead lithium" may even not contain metallic lithium anymore as it has been entirely transformed into SEI-like products. Here, we note that the division into two distinct layers ("live" and "dead") with clearly different properties is rather arbitrary. In reality, many "mixed" situations may appear where the dendritic lithium is partly connected (through finite values of ionic and electronic resistances of SEI) to the bulk lithium. For the sake of clarity, we here keep the established division into two extreme layers ("live" and "dead") and make appropriate comments where necessary.

Dead lithium primarily occurs at the electrolyte side where the passivation reactions are most intense. In terms of transport/reaction mechanism, the properties of "live lithium" and "dead lithium" are essentially different, and these differences constitute the core of present modeling. Interestingly, even if we did not include the more realistic "mixed lithium" case (partially connected lithium), most of the main trends observed experimentally in the present study could be reproduced—as shown in continuation. We note, however, that a more detailed study should allow for a possibility of the existence of "mixed lithium" inside the dendritic structure.

First, we briefly introduce the specific model for pristine, uncycled but passivated lithium (Figure 4). The model is a generalized version of our previous transmission line model[15] consisting of two rails of transistors connected with capacitive elements.

The upper rail (resistors with index ending with "1") describes migration of positive charges (lithium ions) and the lower rail (resistors with index ending with "2") describes migration of negative charges (anions). The parallel combination of both migrations is seen at highest frequencies of impedance response as the well-known "electrolyte resistance".[15]

At lowest frequencies, however, both migrations are coupled through storage in the perpendicular capacitive elements, also known as chemical capacitors.[23] This coupling effectively describes the chemical diffusion process, in electrochemistry also known as Warburg diffusion.

On the right, the transmission line begins in the middle of the separator soaked with bulk electrolyte (elements R_{sep1}, R_{sep2}, and C_{sep}) and continues through the electrolyte in the porous part of SEI (elements R_{por1}, R_{por2}, and C_{por}). Any transport through the solid skeleton of porous SEI is neglected—as the corresponding resistances are many orders of magnitude higher than those across the electrolyte in SEI pores. Upon reaching the compact part of SEI on top of metallic Li, only Li ions can proceed further through it as this layer is conductive for Li^+ only. The resistor due to migration through SEI is denoted as R_{SEI}. Conversely, the lower rail ends up with a capacitive term which indicates that anions cannot pass the SEI. The detailed description of the various possible contributions to this capacitance is beyond the scope of this paper; instead, we assume that the main contribution is due to geometrical capacitance of SEI—hence, it is denoted as C_{SEI}. The charge-transfer resistance due to the reaction between electrons and Li^+ ions is neglected here.

A general impedance response of transmission line in Figure 4b consists of a high-frequency intercept corresponding to electrolyte resistance (because of charge migration in the electrolyte—both in the separator as well as in the pores of SEI). The high-frequency arc is a parallel combination of R_{SEI} and C_{SEI} (highlighted by a red rectangle). The medium-frequency arc is due to chemical diffusion in the electrolyte within the porous part of SEI (green) and the low-frequency arc due to diffusion in the electrolyte-filled separator (blue).

When lithium gets covered with dendrites, the transmission line needs to be modified to account for the more complex transport (Figure 5). In fact, the right part of the transmission line denoted with "SEPARATOR" and "DEAD DENDRITE" retains the previous shape, that is, two simple resistive rails connected with chemical capacitances. However, the left part that refers to processes inside the porous "live lithium" is essentially different compared to the previous simple R_{SEI} and C_{SEI} elements (compare with Figure 4) because now the previous smooth, planar geometry of metallic lithium has transformed into porous lithium. As there is an electrolyte inside the porous lithium, we need additional rails to describe migration and diffusion in the pores of this live lithium (R_{live1}, R_{live2}, and C_{live}). However, in live lithium, the walls of pores are active (an electrochemical reaction can occur there), which needs to be appropriately taken into account. This is a well-known situation from various types of electrochemical devices and has in principle been treated starting with a well-known transmission line by Bisquert.[24] Specifically, one needs to insert perpendicular elements (here simply denoted as R_{SEI} and C_{SEI}) along the diffusional rail. This effectively means that as the ions migrate/diffuse along a pore, they are continuously reacting with its walls. This creates a special shape of impedance response which, in fact, has already been treated analytically.[25,26] In a previous study,[14] we showed that those analytical solutions could be satisfactorily approximated with a transmission line that had essentially the same shape as that proposed in Figure 5 (the part denoted as "LIVE LITHIUM DENDRITE").

The four interconnected processes (three migration/diffusion steps and a reaction along the pores in live dendrites) in transmission line in Figure 5 typically create four arcs and a high-frequency intercept (Figure 5b). The sizes of the four arcs and the HF intercept can be readily evaluated using simple formulas given in the Theoretical Section (Section 3.2). These formulas hold generally, that is, regardless of the values of time constants

DOI: 10.1021/acs.jpcc.9b05887
J. Phys. Chem. C 2019, 123, 27997−28007

(the products of $(R_{j1} + R_{j2})C_j$) of processes "j". In other words, the formulas are the same in the case of well-resolved arcs as shown in the Theoretical Section (Figure 2), or in cases where some arcs are merged because of proximity (similar values) of time constants. An example of a theoretical spectrum with significantly merged low-frequency arcs is shown in Figure 5b, whereas the transition from a well-resolved into a tightly coupled low-frequency spectrum is shown in more detail in Figure S1 (Supporting Information S1). It can be seen that the partial merging of three arcs at lowest frequencies creates an unusual elongated impedance feature which indeed is frequently seen in real measurements involving dendrites (see measurements in continuation of this paper). Having an appropriate model, one can decouple such elongated measured features into individual contributions by different processes, yielding the values of all model parameters, as shown in continuation. Finally, we need to note that the metallic lithium entrapped in dead dendrites, though electrically disconnected from other parts of the conductive electrode, may give rise to a significant additional capacitive term that is expected to affect the measured impedance spectra. In order to keep the transmission line as simple as possible, we did not include this additional capacitive term in the present treatment shown in Figure 5. However, this means that the true values of capacitive terms may be slightly different from those displayed in Tables 1 and S1.

The measured and simulated spectra of pristine lithium using the model in Figure 4 are shown in Figure 6a. Figure 6b shows the other extreme—the measured and simulated (using the model in Figure 5) spectra for lithium anode after prolonged cycling. The spectra differ significantly in all aspects—shape, magnitude, and typical frequencies of different features. However, before analyzing the measured spectra according to the present transmission line models, we first need to comment on the quality of such measurements. We have found that the use of metallic Li is still challenging in terms of reproducibility. We demonstrate our state-of-the-art level of reproducibility by referring to the graphs in the Supporting Information, Section S2. Although the main shape of both graphs is similar (and indeed can be fitted using the same model), there is about 20–25% of difference in the size of the spectra. Also, there are some smaller differences at lowest frequencies. Despite the obvious differences, we wish to note that this is a case of quite good reproducibility with regard to Li electrodes.

In order to further evaluate the quality of typical measurements of cells containing Li electrodes, we carried out a couple of standard tests such as (i) measurements at different values of excitation signal (testing the linearity of response), (ii) repetition of measurements at given steady-state conditions (checking the time invariance of the system), and (iii) Kramers–Kronig analysis (checking whether the system adheres to the principle of causality, see the example of Kramers–Kronig analysis in the Supporting Information, Section S3). The values of model parameters for both simulated spectra shown in Figure 6 are shown in Table 1. The reason for using CPE elements instead of capacitive elements in Figure 6 and Table 1 is explained in more detail in the Theoretical Section (Section 3.4).

One can see that despite the big differences, the parameters describing diffusion in the separator remain more or less the same for both cases. This is expected as the separator should not change significantly during cycling (except in the extreme case when the separator is penetrated by needlelike dendrites creating a short circuit between the electrodes). Using formulas described in the Theoretical Section (Section 3.3), one can also estimate the average chemical diffusion coefficient in separator: 1.9×10^{-10} m^{-2} s. As explained in the Theoretical Section, this value contains implicitly a prefactor for porosity, so care has to be taken when comparing this number to that of a pure electrolyte. Furthermore, the transport number for Li^+ in separator is found to be $t_{Li^+} = 0.14$. In contrast to the separator, very big changes are seen in the resistance and capacitance of the SEI film (R_{SEI} and C_{SEI}). Finally, we need to explain the meaning of parameters R_B and C_C shown in Table 1. R_B represents the resistance of SEI at the bottom of the pore. Its value depends on the surface area at the bottom of pores and also on the properties of the SEI layer. In any case, compared to R_{SEI}, this value will be much bigger as the surface area at the bottom of pores is much smaller than the surface area of the SEI layer on live lithium dendrites. Sensitivity analysis showed that, in fact, if R_B is about 1 order of magnitude higher than R_{SEI}, its contribution to simulated spectra becomes negligible. Accordingly, we merely give an estimated semi-infinite interval for the value of this parameter in Table 1 (and also in Table S1). A similar reasoning for C_C (capacity at the bottom of the pore) leads to a similar semi-infinite interval for this parameter in both tables. A more detailed analysis of parameter values displayed in Table 1 is presented in the Supporting Information (Section S4).

Once we obtain the data for initial (pristine) and final (fully dendrite-covered) lithium surface, we study the intermediate situations. It is known from the literature (and confirmed in the present study) that the initial growth of dendrites on the cycled Li metal surface usually assumes the form of dendritic islands

Table 1. Values of Model Elements Used in Simulation of Spectra Shown in Figure 6a,b

element in model	pristine lithium, Figure 6a (model Figure 2)	fully covered lithium, Figure 6b (model Figure 3)
R_{SEI} [Ω]	119	9
Q_{SEI} [$s^{\alpha_{SEI}}$ Ω^{-1}]	5.9×10^{-6}	7×10^{-5}
R_{por1} [Ω]	6	
R_{por2} [Ω]	2	
Q_{por} [$s^{\alpha_{por}}$ Ω^{-1}]	5.8×10^{-3}	
R_B [Ω]		>90
C_C [F]		$<7 \times 10^{-6}$
R_{live1} [Ω]		60
R_{live2} [Ω]		10
Q_{live} [$s^{\alpha_{live}}$ Ω^{-1}]		6×10^{-2}
R_{dead1} [Ω]		40
R_{dead2} [Ω]		5
Q_{dead} [$s^{\alpha_{dead}}$ Ω^{-1}]	5.8×10^{-2}	0.5
R_{sep1} [Ω]	18	18
R_{sep2} [Ω]	2.5	3
Q_{sep} [$s^{\alpha_{sep}}$ Ω^{-1}]	0.095	0.1
α_{SEI} [a]	0.89	0.85
α_{por}	0.96	
α_{live}		0.95
α_{dead}		0.75
α_{sep}	0.85	0.85

[a] α_k denotes the exponent in the so-called CPE describing the capacitive properties of phase k, that is, $CPE_k = 1/(j\omega)^{\alpha k}Q_k$, where Q_k replaces the corresponding capacitive element C_k.

DOI: 10.1021/acs.jpcc.9b05887
J. Phys. Chem. C 2019, 123, 27997–28007

(ref 27, see also the micrographs in Figure 6c). This means that (depending on the current rate and time of deposition) a significant percentage of the electrode is still similar to the pristine Li electrode's smooth surface (see gray areas in the micrograph of Figure 6c). It is expected that the average properties of such partially covered surface will be a linear combination of pristine and fully dendrite-covered surface. Indeed, the development of electrochemical impedance spectroscopy (EIS) spectra measured during cycling shows similar trends to the mentioned linear combination with progressively larger amount of covered surface (see examples in Figures 6c and S3 in the Supporting Information, Section S4).

To further validate the proposed approach, we carried out additional experiments where we combined the information obtained from impedance measurements with the microscopic observation of surface formations. In particular, we were interested if such a combination could give a new insight into the effects of current density and number of cycles on the electrode surface morphology. The approach is demonstrated on an example of three different cells operated under different conditions (Figure 7).

The left and middle columns in Figure 7 compare the surface morphologies and the corresponding impedance spectra of two electrodes that were cycled using the same current density (0.1 mA cm^{-2}). The left electrode was examined after five cycles (20 h of operation). As indicated, the total thickness of the surface film (live + dead lithium) was about 7 μm. Observations at a larger scale (not shown) indicated that the surface film covered only about 25% of the total surface area, whereas the remaining part consisted of pristine electrodes. This information was taken into account in impedance simulations. The parallel cell was cycled 25 times (100 h of operation) (middle column, Figure 7) using the same current density. Microscopic investigation showed a film that was about 13 μm thick, covering about 95% of the total lithium surface area. Obviously, the film grew both laterally and perpendicularly. The estimated total film volume was about 7 times larger than in the case of 5 cycles, which is slightly more than expected from the total charge flown (5 times more in the case of 25 cycles).

Much more information about the respective dendrite properties, however, can be extracted if we compare the results of simulations of both measured spectra (Figure 7g,h and Table S1 in the Supporting Information). Similarly, as in the case of Figure 6c, we assumed that both measured spectra were linear combinations of the appropriate initial spectrum and an assumed surface that was fully (100%) covered with dendrites (i.e., using the model in Figure 5). As mentioned, we took into account the information that in the case of 5 cycles, 25% of surface was covered with dendrites, whereas after 25 cycles, this percentage was 95%.

Very interestingly (and rather unexpectedly), during simulations, we noticed that many model parameters scaled very well with the thickness of dendrite film. For example, we noticed that when going from 5 cycles (7 μm-thick dendrites) to 25 cycles (13 μm-thick dendrites), all four migration resistances R_{live1}, R_{live2}, R_{dead1}, and R_{dead2} increased roughly by a factor of 2. At the same time, both chemical capacitances (C_{live} and C_{dead}) also increased roughly by a factor of 2, which is close to the increase of dendrite thickness (1.85 times) (note that C_{live} and C_{dead} are directly proportional to the displayed Q_{live} and Q_{dead} as α_{live} is fixed in this case, i.e., it is 0.85 for both 5 and 25 cycle spectrum).

This strongly indicates that the average transport properties of dendrites remained more or less the same during their growth in the course of cycling. In other words, there is no indication that the mechanism of dendrite formation would change from 5th to 25th cycle. By contrast, the values of parameters for SEI film that covers the live dendrites (R_{SEI}, C_{SEI}) showed basically no change from the 5th to the 25th cycle. At a first glance, this is not expected because the total surface area of live dendrites increased by roughly a factor of 2 because of the increase of thickness, so R_{SEI} appropriately decreases and C_{SEI} increases. As this did not happen, we may assume that the SEI film got thicker during cycling—coincidentally by roughly a factor of 2, which annihilated the effect of larger surface area.

Finally, we note that the four migration resistances could also increase because of the shrinkage of the dendrite (live and dead) porosity. However, in this case, the corresponding capacitances (C_{live} and C_{dead}, i.e., Q_{live} and Q_{dead}) should decrease as they are proportional to the volume of space in which diffusion occurs (see eq C3).

As regards, the parameters describing the transport across the electrolyte-filled separator, no noticeable changes were observed. The dynamics of dendrite parameters, however, becomes much more dramatic if we compare Li electrodes cycled at different current densities. The right column in Figure 7 shows a typical surface micrograph together with the measured and simulated spectra of a Li anode that was cycled at a 5 times higher current density than anodes in the left and middle columns of Figure 7. For better comparison, we took care that the total charge transferred during the high-current experiment was the same as the total current transferred during the 25 cycles of the low-current experiment. In other words, only five high-current cycles were performed. Cycling at higher rates resulted in a dendrite layer that was slightly thicker (about 16 μm) than in the case of comparable low-rate cycling (13 μm). However, this thicker film only covered about 50% of the total lithium surface area (as opposed to 95% in the low-rate cycled anode). It seems that at the higher current density, the same amount of transferred charge formed dendrites that were much less uniformly distributed across the Li surface. However, a question remains whether the essential transport/reaction parameters of dendrites are also affected by the current density. This can be answered by comparing the simulated impedance parameters for the high- and low-current density experiment (see Table S1 in the Supporting Information).

First, we compare the transport parameters inside dendrites for both cases. In the case of higher current density, R_{live2} and R_{dead1} are smaller by almost a decade, whereas R_{live1} is smaller by a factor of 1.5 and R_{dead2} does not change significantly. This rather impressive decrease of at least three migration-related resistances (R_{live1}, R_{live2}, and R_{dead1}) is counterintuitive as, in fact, our microscopical investigation showed that the dendrite layer thickness at high rates was even slightly bigger. On the other hand, the respective chemical capacitances (C_{live} and C_{dead}) increased roughly by a factor of 4.5−5 (i.e., by roughly the same factor as the displayed Q_{live} and Q_{dead}). Note that the value of chemical capacitance is proportional to the volume of space where diffusion of mobile carriers occurs (see eq C3 in which the product LA occurs). The much bigger chemical capacitance in the case of higher rates might indicate a bigger average pore size in the dendrites formed at the higher rate. Indeed, this would be consistent with the (much) lower transport resistances, as discussed above.

Next, we compare the values of parameters related to SEI inside live dendrites. Rather strikingly, the high-rate experiment reveals even about 150 times lower R_{SEI} and about 33 times

DOI: 10.1021/acs.jpcc.9b05887
J. Phys. Chem. C 2019, 123, 27997−28007

higher C_{SEI} (Q_{SEI}) value. There are two possible contributions to such changes: either the surface area is much bigger and/or the SEI thickness is much smaller (and may contain more defects).

Based on the examples shown above, we were wondering whether using the present approach, one could provide approximate guidelines that would be used for identification of the main processes occurring during dendritic growth. For example, one could be interested to know what happens with the impedance response when the main processes contributing to cell deterioration are the growth (thickening of the layer) of live porous lithium, the thickening of dead lithium, the electrolyte dry out, and so forth. Indeed, one can show that different hypothetical scenarios will lead to different developments of both the shape of impedance response and its typical magnitude at a given frequency. Figure 8a demonstrates how the measured spectrum shown in Figure 7g would change if the only film growth process was coverage of surface from 25% (solid line, i.e., the actual measurement) to 100% (calculated dotted line). This calculated case of 100% coverage then acts as a reference spectrum to show the other possible effects. Thus, Figure 8b shows the predicted impedance response if the passive film not only covered the Li surface to 100% but at the same time the live porous lithium would get thicker by an arbitrarily chosen factor of 4 (red spectrum). Figure 8c shows a similar scenario—only that not the live lithium but the dead lithium would get thicker by a factor of 4 (green spectrum). Finally, Figure 8d shows the predicted spectrum if the passivation led to electrolyte dry out; specifically, we assumed that after this dry out, only 25% of the electrode surface would still be ionically contacted with the electrolyte.

In terms of the electrode performance, it is important to evaluate how those hypothetical scenarios would affect the total electrode resistance which can be calculated using eq B6 (see the Theoretical Section). It can be seen that just covering the electrode surface by different percentage of dendritic surface (Figure 8a) does not essentially affect the total electrode resistance. This is because coverage with dendrites has two opposite effects: while it slows down the ionic transport toward the active sites on lithium by creating an additional surface layer, it also enhances the reaction kinetics by providing a much larger active surface area (i.e., the surface area of porous live lithium). Because of similar reasons, even thickening of this active surface area of live porous lithium (Figure 8b) does not change the total resistance significantly. By contrast, any increase in the thickness of dead lithium does represents a significant increase in total resistance (in our case, it increases from 137 to 257 Ω, see Figure 8c). Finally, as expected, the effect of electrolyte dry out is highly important—the total electrode resistance is roughly proportional to the percentage of the electrode surface that is wetted with liquid electrolyte.

The scenarios shown in Figure 8 will be rarely seen in their pure form. Very likely, there will be some coexistence/overlap of the effects shown. For example, looking at our results shown in Figure 7 (and checking the values in Table S1), one might say that there is some interplay between the phenomena because the spectra do not follow exactly the patterns shown in Figure 8. Still, one may roughly say that in the case of Figure 7g, the surface coverage is still low (as the second arc is rather small compared to the first and the shape of the first is still not much distorted at high frequencies—in the sense of approaching 45°).

In the other two examples (Figure 7h,i), the shapes and magnitudes point mostly to predominance of the impedance due to transport in live porous lithium. Indeed, this is confirmed by looking at the model values in Table S1, where it is clearly shown that in both cases, the values due to R_{live1} and R_{live1} are significantly higher compared to the values for the other resistors.

Additional phenomena might occur in real electrodes that are not accounted for in this study. Still, the examples shown may act as a rough guideline toward better understanding of the dynamics of Li anodes during cycling as detected by EIS.

5. CONCLUSIONS

A general transmission line model describing the impedance response of metallic lithium in contact with an electrolyte-soaked separator was presented and verified on several sets of measurements. The model is able to describe the main transport/reaction phenomena in pristine (uncycled) metallic lithium covered with SEI as well as more complex phenomena taking place in cycled lithium covered with dendrites of different morphologies. The main advantage of the model (with respect to more rigorous analytical models) is that it can effectively couple different sections of the electrochemical system, for example, processes occurring in the compact part of SEI, processes in porous SEI, phenomena in "live lithium", "dead lithium", and finally, diffusion in the electrolyte-soaked separator. Indeed, it was demonstrated that combinations of these different processes led to the significantly "elongated" low-frequency arc typically observed previously and also typically in this study. Using the present transmission line, this elongated feature can be decoupled into individual contributions in a quantitative way. Even more, we showed that combining the morphological data with impedance spectroscopy measurements, one can formulate a set of simple "rules" that link the essential impedance features of cycled lithium anodes to the underlying physical processes. Such mapping might be of considerable help when trying to identify the main process(ess) contributing to the performance deterioration during cycling of lithium, such as thickening of live porous lithium, thickening of dead lithium, electrolyte dry out, and so forth (see the scheme in Figure 8).

■ ASSOCIATED CONTENT

Supporting Information

The Supporting Information is available free of charge on the ACS Publications website at DOI: 10.1021/acs.jpcc.9b05887.

> Resolving of impedance contributions of the interconnected processes; reproducibility of the EIS measurements; example of Kramers−Kronig analysis on the present measurements; detailed analysis of values shown in Table 1; measured and simulated EIS data at various points during Li stripping and deposition experiment (extension of Figure 6); and values of parameters used in simulations of spectra shown in Figure 7 (PDF)

■ AUTHOR INFORMATION

Corresponding Author

*E-mail: miran.gaberscek@ki.si.

ORCID

Miran Gaberšček: 0000-0002-8104-1693

Author Contributions

This manuscript was written through contributions from all authors. All authors have given approval to the final version of the manuscript.

DOI: 10.1021/acs.jpcc.9b05887
J. Phys. Chem. C 2019, 123, 27997−28007

Notes

The authors declare no competing financial interest.

■ ACKNOWLEDGMENTS

This work was financially supported by Slovene Research Agency and through Helis project (European Union's Horizon 2020 research and innovation program under grant agreement no. 666221).

■ REFERENCES

(1) Peled, E. Lithium Stability and Film Formation in Organic and Inorganic Electrolyte for Lithium Battery Systems. In *Lithium Batteries*; Gabano, J., Ed.; Academic Press, 1983.
(2) Peled, E. The Electrochemical Behavior of Alkali and Alkaline Earth Metals in Nonaqueous Battery Systems—The Solid Electrolyte Interphase Model. *J. Electrochem. Soc.* **1979**, *126*, 2047−2051.
(3) Cheng, X.-B.; Zhang, R.; Zhao, C.-Z.; Zhang, Q. Toward Safe Lithium Metal Anode in Rechargeable Batteries: A Review. *Chem. Rev.* **2017**, *117*, 10403−10473.
(4) Peled, E.; Menkin, S. Review—SEI: Past, Present and Future. *J. Electrochem. Soc.* **2017**, *164*, A1703−A1719.
(5) Cheng, X.-B.; Zhang, R.; Zhao, C.-Z.; Wei, F.; Zhang, J.-G.; Zhang, Q. A Review of Solid Electrolyte Interphases on Lithium Metal Anode. *Adv. Sci.* **2016**, *3*, 1500213.
(6) Nazri, G.; Muller, R. H. Composition of Surface Layers on Li Electrodes in PC, $LiClO_4$ of Very Low Water Content. *J. Electrochem. Soc.* **1985**, *132*, 2050−2054.
(7) Aurbach, D.; Daroux, M. L.; Faguy, P. W.; Yeager, E. Identification of Surface Films Formed on Lithium in Propylene Carbonate Solutions. *J. Electrochem. Soc.* **1987**, *134*, 1611−1620.
(8) Dey, A. N. Lithium Anode Film and Organic and Inorganic Electrolyte Batteries. *Thin Solid Films* **1977**, *43*, 131−171.
(9) Peled, E. Film Forming Reaction at the Lithium/Electrolyte Interface. *J. Power Sources* **1983**, *9*, 253−266.
(10) Aurbach, D.; Zaban, A.; Schechter, A.; Ein-Eli, Y.; Zinigrad, E.; Markovsky, B. The Study of Electrolyte Solutions Based on Ethylene and Diethyl Carbonates for Rechargeable Li Batteries. *J. Electrochem. Soc.* **1995**, *142*, 2873−2882.
(11) Aurbach, D.; Ein-Ely, Y.; Zaban, A. The Surface Chemistry of Lithium Electrodes in Alkyl Carbonate Solutions. *J. Electrochem. Soc.* **1994**, *141*, L1−L3.
(12) Aurbach, D.; Zinigrad, E.; Cohen, Y.; Teller, H. A Short Review of Failure Mechanisms of Lithium Metal and Lithiated Graphite Anodes in Liquid Electrolyte Solutions. *Solid State Ionics* **2002**, *148*, 405−416.
(13) Wood, K. N.; Kazyak, E.; Chadwick, A. F.; Chen, K.-H.; Zhang, J.-G.; Thornton, K.; Dasgupta, N. P. Dendrites and Pits: Untangling the Complex Behavior of Lithium Metal Anodes through Operando Video Microscopy. *ACS Cent. Sci.* **2016**, *2*, 790−801.
(14) Drvarič Talian, S.; Moškon, J.; Dominko, R.; Gaberšček, M. Impedance Response of Porous Carbon Cathodes in Polysulfide Redox System. *Electrochim. Acta* **2019**, *302*, 169−179.
(15) Adamič, M.; Drvarič Talian, S.; Sinigoj, A. R.; Humar, I.; Moškon, J.; Gaberšček, M. A Transmission Line Model of Electrochemical Cell's Impedance: Case Study on a Li-S System. *J. Electrochem. Soc.* **2019**, *166*, A5045−A5053.
(16) Drvarič Talian, S.; Moškon, J.; Dominko, R.; Gaberšček, M. Reactivity and Diffusivity of Li Polysulfides: A Fundamental Study Using Impedance Spectroscopy. *ACS Appl. Mater. Interfaces* **2017**, *9*, 29760−29770.
(17) Keddam, M.; Mattos, O. R.; Takenouri, H. Reaction Model for Iron Dissolution Studied by Electrode Impedance: I. Experimental Results and Reaction Model. *J. Electrochem. Soc.* **1981**, *128*, 257−266.
(18) Macdonald, D. D.; Real, S.; Smedley, S. I.; Urquidi-Macdonald, M. Evaluation of Alloy Anodes for Aluminum-Air Batteries: IV. Electrochemical Impedance Analysis of Pure Aluminum in Formula at 25°C. *J. Electrochem. Soc.* **1988**, *135*, 2410−2414.
(19) Park, M. S.; Ma, S. B.; Lee, D. J.; Im, D.; Doo, S.-G.; Yamamoto, O. A Highly Reversible Lithium Metal Anode. *Sci. Rep.* **2015**, *4*, 3815−3822.
(20) Steiger, J.; Kramer, D.; Mönig, R. Microscopic Observations of the Formation, Growth and Shrinkage of Lithium Moss during Electrodeposition and Dissolution. *Electrochim. Acta* **2014**, *136*, 529−536.
(21) Tang, C.-Y.; Dillon, S. J. In Situ Scanning Electron Microscopy Characterization of the Mechanism for Li Dendrite Growth. *J. Electrochem. Soc.* **2016**, *163*, A1660−A1665.
(22) Sano, H.; Kitta, M.; Matsumoto, H. Effect of Charge Transfer Resistance on Morphology of Lithium Electrodeposited in Ionic Liquid. *J. Electrochem. Soc.* **2016**, *163*, D3076−D3079.
(23) Jamnik, J.; Maier, J.; Pejovnik, S. A Powerful Electrical Network Model for the Impedance of Mixed Conductors. *Electrochim. Acta* **1999**, *44*, 4139−4145.
(24) Bisquert, J. Influence of the Boundaries in the Impedance of Porous Film Electrodes. *Phys. Chem. Chem. Phys.* **2000**, *2*, 4185−4192.
(25) Devan, S.; Subramanian, V. R.; White, R. E. Analytical Solution for the Impedance of a Porous Electrode. *J. Electrochem. Soc.* **2004**, *151*, A905−A913.
(26) Huang, J.; Zhang, J. Theory of Impedance Response of Porous Electrodes: Simplifications, Inhomogeneities, Non-Stationarities and Applications. *J. Electrochem. Soc.* **2016**, *163*, A1983−A2000.
(27) Rehnlund, D.; Ihrfors, C.; Maibach, J.; Nyholm, L. Dendrite-Free Lithium Electrode Cycling via Controlled Nucleation in Low LiPF6 Concentration Electrolytes. *Mater. Today* **2018**, *21*, 1010−1018.

DOI: 10.1021/acs.jpcc.9b05887
J. Phys. Chem. C 2019, 123, 27997−28007